JACS
JOURNAL OF THE AMERICAN CHEMICAL SOCIETY
pubs.acs.org/JACS
Article

Noncovalent Liquid Phase Functionalization of 2H-WS_2 with PDI: An Energy Conversion Platform with Long-Lived Charge Separation

Tobias Scharl,[#] Gerhard Binder,[#] Xin Chen, Tadahiro Yokosawa, Alejandro Cadranel, Kathrin C. Knirsch, Erdmann Spiecker, Andreas Hirsch,* and Dirk M. Guldi*

Cite This: *J. Am. Chem. Soc.* 2022, 144, 5834–5840
Read Online
ACCESS | Metrics & More | Article Recommendations | Supporting Information

ABSTRACT: Transition metal dichalcogenides are attractive 2D materials in the context of solar energy conversion. Previous investigations have focused predominantly on the properties of these systems. The realization of noncovalent hybrids with, for example, complementary electroactive materials remains underexplored to this date for exfoliated WS_2. In this contribution, we explore WS_2 by means of exfoliation and integration together with visible light-absorbing and electron-accepting perylene diimides into versatile electron-donor acceptor hybrids. Important is the distinct electron-donating feature of WS_2. Detailed spectroscopic investigations of **WS_2–PDI** confirm the electron donor/acceptor nature of the hybrid and indicate that green light photoexcitation leads to the formation of long-lived **$WS_2^{\bullet+}$–$PDI^{\bullet-}$** charge-separated states.

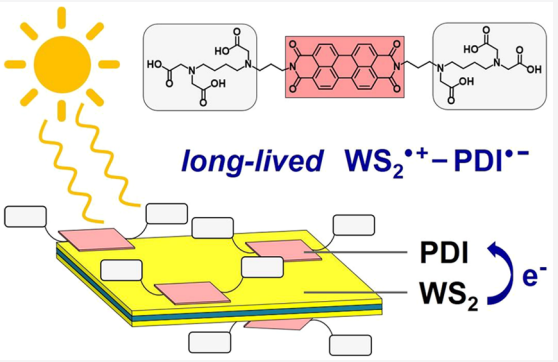

INTRODUCTION

In the last decade, two-dimensional (2D) materials have attracted huge interest owing to their atomically thin geometry. Tungsten disulfide (WS_2), albeit less explored than molybdenum disulfide (MoS_2), is a typical example of layered transition metal dichalcogenides (TMDs). WS_2 adopts a hexagonal, layered structure similar to the aforementioned MoS_2 with the metal atom in a triagonal prismatic coordination, sandwiched between two atomic layers of sulfur atoms. As such, strong in-plane covalent W–S bonds are combined with weak van der Waals couplings between neighboring layers. By virtue of weak interlayer interactions, bulk WS_2 is easily exfoliated to yield few layer or monolayer WS_2.[1]

Chemical exfoliation of TMDs by means of intercalation-assisted exfoliation in liquids commonly generates large quantities of single layers. Most notable is the well-known use of *n*-butyllithium dissolved in hexane.[2] Intercalation with alkali metals alters, however, the monolayers with respect to their structure and, thus, their properties. As a matter of fact, upon this treatment, the thermodynamically stable, semiconducting 2H-phase (trigonal prismatic) is converted into the metastable, metallic 1T-phase (distorted octahedral). However, semiconducting 2H-WS_2 is maintained if sonication-assisted liquid-phase exfoliation of bulk WS_2 is employed. In this case, suitable organic solvents or water in the presence of surfactants are needed.[3] Designed centrifugation approaches allow us to obtain monolayers with improved yields.[4]

As one of the key characteristics, monolayer 2H-WS_2 is a direct-gap semiconductor (~2.0 eV), contrary to its bulk counterpart with its indirect band gap (~1.3 eV).[5] The electrical, optical, and transport properties of 2H-WS_2 pronouncedly depend on the stacking of the WS_2 sheets, which can be exploited for tuning these properties. Controlling the electronic behavior of WS_2, which is governed by excitonic transitions, is mandatory for the realization of energy conversion devices. Importantly, molecular chemistry approaches are uniquely suited to address the aforementioned.[6−9]

Noncovalent interactions assist in tailoring the properties of nanomaterials. This was first explored for graphene[10] and later transferred to inorganic analogs, such as black phosphorus[11] and MoS_2[12] as the representative of TMDs. Noncovalent functionalization of TMDs has predominantly been established on surfaces, except for few exceptions.[13,14] Leading examples are chemical vapor deposition grown MoS_2 and tungsten diselenide (WSe_2).[15] Studies in the liquid phase remain elusive. A combined approach, that is covalent and noncovalent bonds in dispersion, was shown for MoS_2 and WS_2 *via* defect functionalization and electrostatic interactions with porphyrins.[16] A theoretical work on noncovalent interactions of WS_2 was implemented for small fullerenes (B_{12} and C_{20})[17] as well as NH_3 and H_2O molecules.[18]

Received: November 12, 2021
Published: March 26, 2022

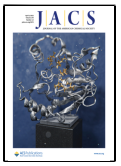

Herein, we report for the first time on the noncovalent liquid phase functionalization of 2H-WS_2. As a suitable organic ligand (OL) allowing to bind *via* pronounced σ (WS_2)−π (OL) stacking interactions, we opted for an ethylenediaminetetraacetic acid (EDTA) perylene diimides (**PDI**) derivative (see Figure S1, left and Scheme 1), which is known from the literature.[19] What stands out among PDIs are their strong light harvesting and good electron accepting features.[20] Leading examples are **PDI**-based noncovalent functionalization of 2D materials like graphene, boron nitride, black phosphorous,[21] and also 3D TMDs. At the same time, the binding to WS_2 should be facilitated by electron donor−acceptor interactions between WS_2 and **PDI**, in addition to stacking. Importantly, it has been demonstrated that TMDs are complementary electron donors, which were integrated into covalently linked MoS_2-PDI conjugates.[22] As a consequence, we expected a robust photoenergy conversion platform. Our WS_2−**PDI** hybrid was comprehensively characterized by spectroscopic methods, and *inter alia* we gathered insights into the electronic interactions between WS_2 and **PDI** upon photoexcitation on the femto- to nanosecond timescales.

Scheme 1. Illustration of the Sonication-Assisted Liquid Phase Exfoliation of Bulk 2H-WS_2 (Composed of Three-Atomic S−W−S Sandwich Layers) with Sodium Cholate (Shown as Blue Spheres) and the Subsequent Noncovalent Functionalization of the Purified WS_2 Nanosheets with PDI (Core in Red and Side Groups in Gray) in an Aqueous Solution Resulting in WS_2−PDI

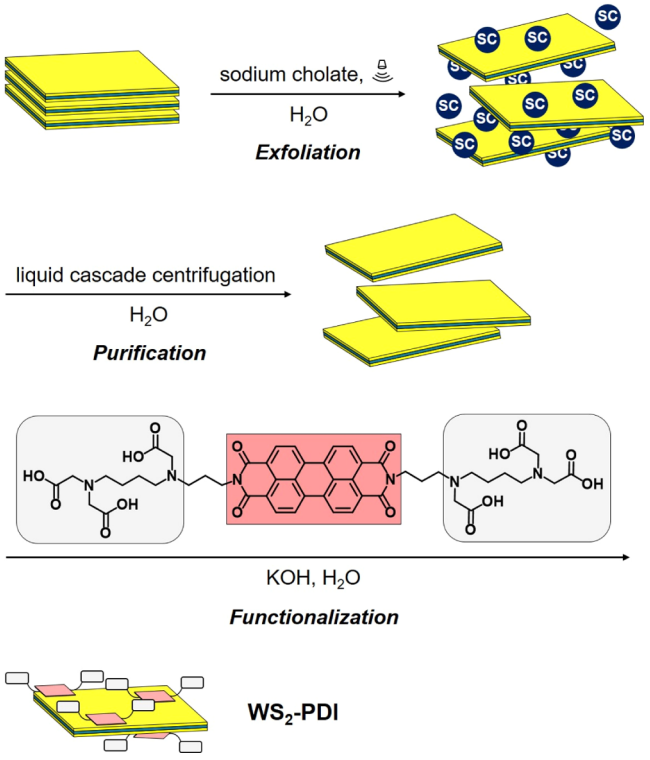

RESULTS

Exfoliated WS_2 nanosheets were produced by probe sonication of commercially available WS_2 powder in water, utilizing sodium cholate (SC) as a stabilizing surfactant. The resulting polydisperse dispersion of WS_2 nanosheets was purified *via* multiple centrifugations with varying rotational speed, as previously described.[4] The few layer material was further processed by successive washing with water to remove the SC surfactant and followed by centrifugation-induced precipitation. The WS_2 nanosheets were then redispersed in an aqueous solution of **PDI**, stirred for 1 h, and finally centrifuged to afford WS_2−**PDI** (see Figure S1, right and Scheme 1).

PDI (see Figure S1, left) is water soluble under slightly basic conditions and was dissolved in a potassium hydroxide (KOH) solution (pH ≈ 10).[19] Absorption spectroscopy corroborates the aggregation of **PDI** in solution due to intermolecular π−π stacking interactions. In Figure S2 (black absorption spectrum with the typical features of **PDI**), the ratio between the (0,0)- and (0,1)-absorptions at 542 and 501 nm, respectively, is around 0.55, suggesting predominantly aggregated species in solution.[19] The absorption spectrum of WS_2 (see Figure 1, black curve) is characterized by three excitonic transitions, namely, the A, B, and C excitons at 623, 520 (shoulder), and 337 nm, respectively.[23] The absorption spectrum of WS_2−**PDI** reveal the WS_2 excitonic bands, but the absence of any **PDI** characteristics (see Figure 1, red curve). As a matter of fact, the **PDI**-centered absorbance is only discernible in the form of an intensity increase of the 520 nm shoulder. Interestingly, in addition to the excitonic WS_2 features, WS_2−**PDI** gives rise to a new transition at 571 nm. We assign this to a charge-transfer (CT) band, which is 29 nm red-shifted compared to the (0,0)-absorption of the **PDI** reference. This suggests strong electron donor/acceptor electronic interactions in the ground state.[a] Please note that covalently linked MoS_2-PDI conjugates fail to exhibit similar CT bands or any evidence for intercomponent ground-state electronic coupling.[22] A likely rationale is centered around the noncovalent nature of WS_2−**PDI**. Here, **PDI**s are accommodated at positions, where the electronic interactions with WS_2 are maximized. According to the second derivative of the absorption spectrum (see Figure 1, inset), the WS_2 excitonic bands lack any appreciable shifts upon functionalization. Similar conclusions were drawn for a previously reported covalent MoS_2−PDI conjugate.[22] It signifies that the degree of functionalization is insufficient to significantly alter Coulomb interactions between electrons and holes within WS_2 *via* dielectric screening.[24]

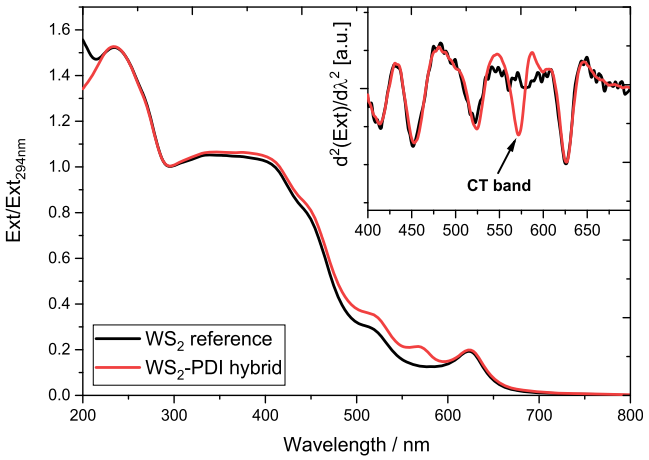

Figure 1. Normalized absorption spectra of WS_2 (black) and WS_2−**PDI** (red). Inset: second derivative of the absorption spectra.

Concerning the polydispersity of the WS_2 nanosheets in lateral size and thickness, it has recently been shown that

https://doi.org/10.1021/jacs.1c11977
J. Am. Chem. Soc. 2022, 144, 5834−5840

absorption spectra allow for the simultaneous quantification of the nanosheets dimensions in dispersion.[25] The average length $\langle L \rangle$ (longest dimension) and layer number $\langle N \rangle$ of the exfoliated **WS_2** were determined to be $\langle L \rangle$ = 60 nm (Ext ratio 235/295 = 1.5) and $\langle N \rangle$ = 3.5 (A exciton centered at 624.5 nm), respectively. By means of high-angle annular dark-field scanning transmission electron microscopy (HAADF STEM) measurements, we probed the morphology of **WS_2–PDI** (see Figure S3). Even though the flakes exhibit a rather broad size distribution from 20 to 100 nm, the average layer number was determined to be $\langle N \rangle$ = 3.5.

Strong interactions between **WS_2** and **PDI** were further corroborated by Raman spectroscopy. Of great importance is the strong quenching of the **PDI** fluorescence in **WS_2–PDI**. The Raman spectrum (see Figure 2, red spectrum) shows the

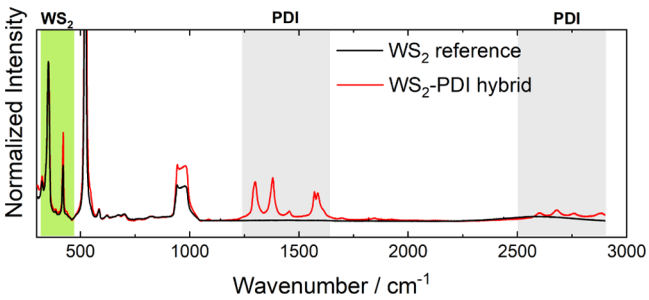

Figure 2. Raman spectra of **WS_2** reference (black) and **WS_2–PDI** (red).

WS_2 characteristics, namely, the 2LA(M) mode at 352 cm^{-1} (overlapping with the first order $^1E_{2g}(\Gamma)$ mode at 356 cm^{-1}) and the $A_{1g}(\Gamma)$ mode at 418 cm^{-1}, in line with the **WS_2** reference (see Figure 2, black spectrum).[26] Additionally, the **PDI** vibrational modes in **WS_2–PDI** appear at 1301/1380 cm^{-1} (in-plane ring "breathing"), 1456 cm^{-1} (ring deformation), 1573/1588 cm^{-1} (in-plane C–C stretching), and 1699 cm^{-1} (imide bending), as well as the imide Raman bands of the branched EDTAs between 2600 and 3200 cm^{-1}. All of the aforementioned proves the successful functionalization of **WS_2** and the formation of **WS_2–PDI**.

Furthermore, fluorescence spectroscopy provided valuable insights into the electronic communication in the excited state within **WS_2–PDI**. Dispersed **WS_2** nanosheets in water (see Figure 3, left) show weak photoluminescence (PL) at 612 nm (2.03 eV), when photoexcited between 340 and 460 nm. This is attributed to the direct-gap PL of a **WS_2** monolayer.[27] It should be noted that the quantum efficiency of the **WS_2** PL is dependent on the number of layers. The direct excitonic transition at the K point is energetically favored for monolayers. With the increasing number of layers, the indirect transition from the T point of the conduction band to the Γ point of the valence band becomes energetically favored and leads to a dramatic decrease of the PL quantum efficiency.[27] Here, the **WS_2** PL in the reference spectrum indicates the presence of a high monolayer content in the dispersion. Interestingly, after the addition of **PDI** to the exfoliated **WS_2**, we observed a strong fluorescence quenching of the **WS_2** PL (see Figure 3, right). This quenching was seen for heterojunctions comprising a 3,4,9,10-perylene tetracarboxylic dianhydride thin film deposited onto a **WS_2** monolayer.[28] The PL quenching rate of **WS_2** excitons was determined to be 81 ± 2%, which is highly consistent with the data presented by Liu *et al.*[28] Our PL quenching is attributed to a charge transfer process across the **WS_2–PDI** interface (*vide infra*).

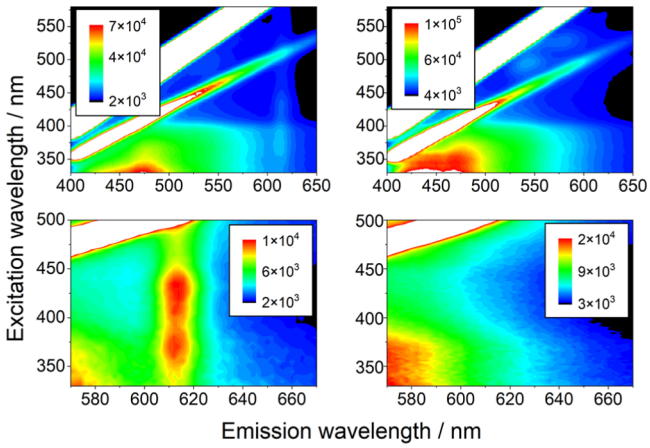

Figure 3. Top: 2D PL mapping of **WS_2** reference (left) with a PL maximum at 612 nm and **WS_2–PDI** (right) with a quenched PL. Bottom: magnification around the 612 nm region, for **WS_2** reference (left) and **WS_2–PDI** (right).

The steady-state fluorescence spectrum of **PDI** shows maxima at 543 and 586 nm (see Figure S2). Due to aggregation, the fluorescence quantum yield is with 0.26 notably lower than that for nonaggregated **PDI**.[29] In stark contrast, **WS_2–PDI** (see Figure 3, right) is nearly non-fluorescent. This is a consequence of strong intercomponent electronic interactions in the excited state, which opens additional nonradiative decay channels absent in **PDI**.[b]

We then turned to femtosecond transient absorption spectroscopy (fs-TAS) in water and at room temperature. fs-TAS of the **PDI** reference upon 500 nm photoexcitation leads to strong ground-state bleaching at around 480 nm as well as photoinduced absorptions at 539 and 600 nm, which reach all the way to 1000 nm. Global analysis of the data was based on a three-species sequential kinetic model (see Figure S4). The respective lifetimes are 3.8 ps, 271 ps, and 3.3 ns. The spectral shape of the first two species is fairly similar with a 480 nm minimum and 538, 600, 700, 785, and 817 nm maxima. Both states are ascribed to **PDI** aggregates: the first species is a vibronically excited hot-S_1 and the second species is the vibronically relaxed S_1. The third species, which is ascribed to the fluorescent S_1 of nonaggregated **PDI**, features minima at 471, 540, and 590 nm as well as maxima at 700 and 930 nm. The minima correspond to the ground-state absorption and stimulated emission, respectively.[30]

In the case of the **WS_2** reference, 500 nm photoexcitation leads to ground-state bleaching of exfoliated **WS_2** at 420, 517, and 620 nm together with the formation of positive absorptions at 465, 540, and 640 nm (see Figure S5). Global analysis was carried out, using a model, which resembles the dynamics already established in the analysis of other TMDs, such as MoS_2.[31,32] By virtue of this model, five exponential decays with lifetimes of 0.4, 2, 21, and 129 ps were deconvoluted. Notably, the fifth and final species is persistent on the timescale of our fs-TAS experiments. The aforementioned states include, respectively, the exciton generation (eg), biexciton (be), and trion (tr) formation as well as the decay of these many-body particles into single excitons (se) followed by excitons that diffuse across the layers in *z*-direction (de) before they recombine and recover the ground state.

https://doi.org/10.1021/jacs.1c11977
J. Am. Chem. Soc. 2022, 144, 5834–5840

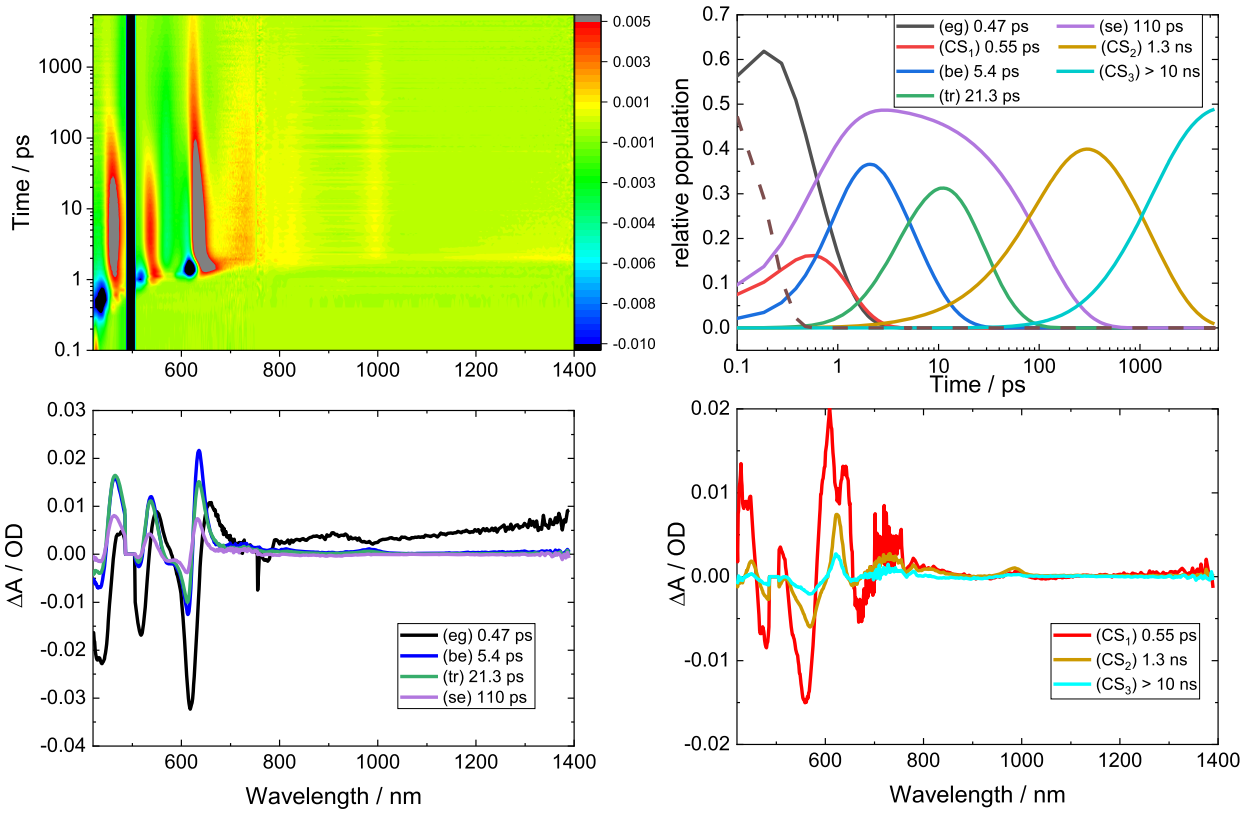

Figure 4. Top left: 3D differential absorption heat map obtained upon 500 nm photoexcitation in fs-TAS with **WS_2–PDI**, in water and at room temperature. Top right: Concentration evolution as a function of time. Bottom left: Species-associated spectra of the **WS_2**-related states in **WS_2–PDI**. Bottom right: Species-associated spectra of the CS states in **WS_2–PDI**.

At first glance, the transient absorption spectra of **WS_2–PDI**, similar to the ground-state absorption, are dominated by **WS_2**-related features in the visible range. In the near-infrared range, a closer look at the 3D differential absorption heat map assists in revealing a sharp positive signal at 986 nm (see Figure 4, top left panel). This feature is **PDI** centered and of utmost importance as it is the fingerprint absorption of the one-electron reduced form of **PDI**, **$PDI^{\bullet-}$**.[23] It is subject to a slow decay throughout the femtosecond and nanosecond timescales (please see nanosecond transient absorption spectroscopy (ns-TAS) experiments in Figures 4, S6, and S7). From its presence, we conclude the coexistence of **WS_2**-centered excited states, on the one hand, and charge-separated (CS) states, on the other hand. To account for this fact, target analysis required an elaborated kinetic model to fit the data (see Figures 4 and 5). The model is based on the parallel decay of two different branches. At the origin of these two branches is the **WS_2** (eg) state, which is formed upon light absorption. It consists of the **WS_2**-related features (see Figure 4, bottom left panel, black curve), namely, minima at 430, 517, 620 nm, maxima at 480, 550, 657 nm, and a broad feature stretching from 990 to 1400 nm. It is within 0.5 ps that the **WS_2** (eg) state deactivates in parallel *via* two different branches—vide infra.

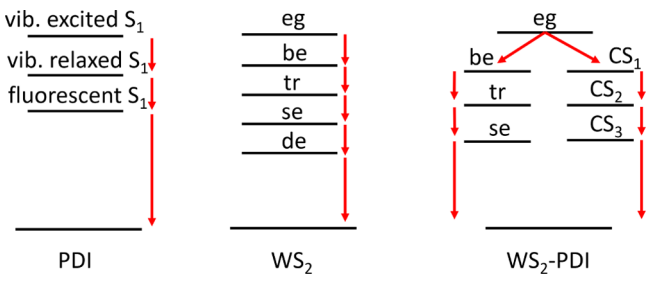

Figure 5. Kinetic models used to fit the fs-TAS and ns-TAS data of **PDI**, **WS_2**, and **WS_2–PDI** on the left, in the center, and on the right, respectively.

One of these two branches relates to **WS_2**-centered excited states and dynamics thereof. It features three different states with lifetimes of 5.4 ps (blue), 21 ps (green), and 110 ps (purple), respectively (see Figure 4. Their spectral shapes as well as their lifetimes, bottom left and top right panel) are in sound agreement with be, tr, and se, respectively. Our assignments are based on the conclusions, which were drawn from the experiments performed with the **WS_2** reference—*vide supra*. Importantly, no sizeable **PDI**-related absorptions are discernible across the visible range for these excited states. This confirms their nature as an exclusive **WS_2**-centered species. The second branch consists likewise of three species (see Figure 4, top right panel). In this instance, the respective lifetimes are 0.6 ps (red), 1.3 ns (yellow), and >10 ns (cyan). What is common to all three of them is their spectral signatures (see Figure 4, bottom right panel). However, they differ from those observed for the **WS_2**- and **PDI** references. The most prominent characteristics are minima at 480 and 568 nm, a broad maximum around 730 nm, and a sharp maximum at 986 nm. Notable is the fact that the 568 nm minimum mirror images the CT absorption seen in the ground state, while the remaining features resemble the fingerprint absorption of the one-electron reduced form of **PDI**.[33] In other words, our target analysis underscores the formation of

https://doi.org/10.1021/jacs.1c11977
J. Am. Chem. Soc. 2022, 144, 5834−5840

$WS_2^{\bullet+}$−$PDI^{\bullet-}$ CS states evolving between the electron-donating WS_2 and the electron-accepting **PDI**.

To study the charge-recombination dynamics in detail, ns-TAS was deemed necessary. Figure S7 shows the 3D differential absorption heat map and global fits of the data. Two species with nearly identical differential spectra were deconvoluted. Their lifetimes are 6 and 162 ns, respectively.[c] Both species are in agreement with the fs-TAS analyses and assigned to the $WS_2^{\bullet+}$−$PDI^{\bullet-}$ CS states. It is interesting to note that only the latter species reinstates the ground state *via* charge recombination.

Single wavelength analyses involving the fingerprint absorptions of $PDI^{\bullet-}$ reveal a multiexponential decay on a timescale of up to several hundred nanoseconds (see Figures S6 and S7). Such a finding is rationalized on grounds of further separating the charges in the $WS_2^{\bullet+}$−$PDI^{\bullet-}$ CS state. Very likely is that the positively charged hole on the WS_2 electron donor is subject to charge-shifting *via* hopping. In light of the latter, the initially formed CS state (CS_1) transforms *via*, for example, a charge shift into a second CS state (CS_2), in which the charges are more spatially separated from each other. As such, CS_1 yields sequentially CS_2 and the third CS state (CS_3) within 0.6 and 1.3−6.0 ns, respectively, before charge recombination takes over. Remarkable is that it takes 162 ns until the ground state is recovered from CS_3 (see Figure S7). Given the almost linear decay of the 986 nm signal, it is likely that other different CS states with different electron−hole distances and therefore also different lifetimes are present in WS_2−**PDI**.[d]

CONCLUSIONS

In conclusion, we succeeded for the very first time in synthesizing a WS_2−**PDI** hybrid by linking electron-donating, exfoliated WS_2 to **PDI**, which serves as a light harvester and electron acceptor. Thoroughly performed characterization revealed the successful formation of WS_2−**PDI**. In the ground state, a CT absorption, which stems from strong electronic communication, is only discernible in WS_2−**PDI**, but not in the individual components. These strong electronic interactions result in the excited state in the population of a long-lived (162 ns) $PDI^{\bullet-}$−$WS_2^{\bullet+}$ CS state. Our results prompt to explore WS_2−**PDI** hybrids in catalytic schemes. To this end, the long-lived nature of the CS states should be employed to drive subsequent charge shifts to catalytically active reaction centers.

ASSOCIATED CONTENT

Supporting Information

The Supporting Information is available free of charge at https://pubs.acs.org/doi/10.1021/jacs.1c11977.

Materials and instrumental technique details, synthetic procedures, and additional figures, including HAADF STEM images, 3D-fluorescence map, fs-TAS, and ns-TAS spectra (PDF)

AUTHOR INFORMATION

Corresponding Authors

Andreas Hirsch − *Department of Chemistry and Pharmacy, Friedrich-Alexander-Universität (FAU) Erlangen-Nürnberg, 91058 Erlangen, Germany;* orcid.org/0000-0003-1458-8872; Email: andreas.hirsch@fau.de

Dirk M. Guldi − *Department of Chemistry and Pharmacy, Interdisciplinary Center for Molecular Materials, Friedrich-Alexander-Universität (FAU) Erlangen-Nürnberg, 91058 Erlangen, Germany;* orcid.org/0000-0002-3960-1765; Email: dirk.guldi@fau.de

Authors

Tobias Scharl − *Department of Chemistry and Pharmacy, Interdisciplinary Center for Molecular Materials, Friedrich-Alexander-Universität (FAU) Erlangen-Nürnberg, 91058 Erlangen, Germany*

Gerhard Binder − *Department of Chemistry and Pharmacy, Friedrich-Alexander-Universität (FAU) Erlangen-Nürnberg, 91058 Erlangen, Germany*

Xin Chen − *Department of Chemistry and Pharmacy, Friedrich-Alexander-Universität (FAU) Erlangen-Nürnberg, 91058 Erlangen, Germany*

Tadahiro Yokosawa − *Institute of Micro- and Nanostructure Research, and Center for Nanoanalysis and Electron Microscopy (CENEM), IZNF, Friedrich-Alexander-Universität (FAU) Erlangen-Nürnberg, 91058 Erlangen, Germany*

Alejandro Cadranel − *Department of Chemistry and Pharmacy, Interdisciplinary Center for Molecular Materials, Friedrich-Alexander-Universität (FAU) Erlangen-Nürnberg, 91058 Erlangen, Germany; Facultad de Ciencias Exactas y Naturales, Departamento de Química Inorgánica, Analítica y Química Física, Universidad de Buenos Aires, C1428EHA Buenos Aires, Argentina; CONICET−Universidad de Buenos Aires. Instituto de Química Física de Materiales, Medio Ambiente y Energía (INQUIMAE), C1428EHA Buenos Aires, Argentina;* orcid.org/0000-0002-6597-4397

Kathrin C. Knirsch − *Department of Chemistry and Pharmacy, Friedrich-Alexander-Universität (FAU) Erlangen-Nürnberg, 91058 Erlangen, Germany*

Erdmann Spiecker − *Institute of Micro- and Nanostructure Research, and Center for Nanoanalysis and Electron Microscopy (CENEM), IZNF, Friedrich-Alexander-Universität (FAU) Erlangen-Nürnberg, 91058 Erlangen, Germany;* orcid.org/0000-0002-2723-5227

Complete contact information is available at: https://pubs.acs.org/10.1021/jacs.1c11977

Author Contributions

[#]T.S. and G.B. contributed equally to this work.

Notes

The authors declare no competing financial interest.

ACKNOWLEDGMENTS

This project has received funding from the European Union's Horizon 2020 research and innovation programme Graphene Flagship under grant agreement No 881603. Additional support is acknowledged from the Excellence Cluster "Engineering of Advanced Materials". A.C. is part of the research staff of CONICET and a member of ALN.

ADDITIONAL NOTES

[a]Aggregation impeded, however, gathering electrochemical information as a means to complement the investigation of the ground-state electronic interactions.

[b]However, the fact that fluorescence stemming from **PDI** occurs despite thoroughly washing of the samples with water

several times, demonstrates the noncovalent binding of the organic molecule to the TMD.
[c]We correlate the 6 and 162 ns components from ns-TAS with the 1.3 and >10 ns components from fs-TAS.
[d]Our kinetic model includes the minimum number of CS states needed to adequately describe the experimental observations.

REFERENCES

(1) Chhowalla, M.; Shin, H. S.; Eda, G.; Li, L.-J.; Loh, K. P.; Zhang, H. The Chemistry of Two-Dimensional Layered Transition Metal Dichalcogenide Nanosheets. *Nat. Chem.* **2013**, *5*, 263−275.
(2) Knirsch, K. C.; Berner, N. C.; Nerl, H. C.; Cucinotta, C. S.; Gholamvand, Z.; McEvoy, N.; Wang, Z.; Abramovic, I.; Vecera, P.; Halik, M.; Sanvito, S.; Duesberg, G. S.; Nicolosi, V.; Hauke, F.; Hirsch, A.; Coleman, J. N.; Backes, C. Basal-Plane Functionalization of Chemically Exfoliated Molybdenum Disulfide by Diazonium Salts. *ACS Nano* **2015**, *9*, 6018−6030.
(3) Nicolosi, V.; Chhowalla, M.; Kanatzidis, M. G.; Strano, M. S.; Coleman, J. N. Liquid Exfoliation of Layered Materials. *Science* **2013**, *340*, 1226419.
(4) Backes, C.; Szydłowska, B. M.; Harvey, A.; Yuan, S.; Vega-Mayoral, V.; Davies, B. R.; Zhao, P.-l.; Hanlon, D.; Santos, E. J. G.; Katsnelson, M. I.; Blau, W. J.; Gadermaier, C.; Coleman, J. N. Production of Highly Monolayer Enriched Dispersions of Liquid-Exfoliated Nanosheets by Liquid Cascade Centrifugation. *ACS Nano* **2016**, *10*, 1589−1601.
(5) Gusakova, J.; Wang, X.; Shiau, L. L.; Krivosheeva, A.; Shaposhnikov, V.; Borisenko, V.; Gusakov, V.; Tay, B. K. Electronic Properties of Bulk and Monolayer TMDs: Theoretical Study Within DFT Framework (GVJ-2e Method). *Phys. Status Solidi A* **2017**, *214*, 1700218.
(6) Hirsch, A.; Hauke, F. Post-Graphene 2D Chemistry: The Emerging Field of Molybdenum Disulfide and Black Phosphorus Functionalization. *Angew. Chem., Int. Ed.* **2018**, *57*, 4338−4354.
(7) Bertolazzi, S.; Gobbi, M.; Zhao, Y.; Backes, C.; Samorì, P. Molecular Chemistry Approaches for Tuning the Properties of Two-Dimensional Transition Metal Dichalcogenides. *Chem. Soc. Rev.* **2018**, *47*, 6845−6888.
(8) Brill, A. R.; Koren, E.; de Ruiter, G. Molecular Functionalization of 2D Materials: From Atomically Planar 2D Architectures to off-Plane 3D Functional Materials. *J. Mater. Chem. C* **2021**, *9*, 11569−11587.
(9) Stergiou, A.; Tagmatarchis, N. Molecular Functionalization of Two-Dimensional MoS_2 Nanosheets. *Chem. - Eur. J.* **2018**, *24*, 18246−18257.
(10) Kozhemyakina, N. v.; Englert, J. M.; Yang, G.; Spiecker, E.; Schmidt, C. D.; Hauke, F.; Hirsch, A. Non-Covalent Chemistry of Graphene: Electronic Communication with Dendronized Perylene Bisimides. *Adv. Mater.* **2010**, *22*, 5483−5487.
(11) Abellán, G.; Lloret, V.; Mundloch, U.; Marcia, M.; Neiss, C.; Görling, A.; Varela, M.; Hauke, F.; Hirsch, A. Noncovalent Functionalization of Black Phosphorus. *Angew. Chem.* **2016**, *128*, 14777−14782.
(12) Molina-Mendoza, A. J.; Vaquero-Garzon, L.; Leret, S.; de Juan-Fernández, L.; Pérez, E. M.; Castellanos-Gomez, A. Engineering the Optoelectronic Properties of MoS_2 Photodetectors through Reversible Noncovalent Functionalization. *Chem. Commun.* **2016**, *52*, 14365−14368.
(13) Nguyen, E. P.; Carey, B. J.; Harrison, C. J.; Atkin, P.; Berean, K. J.; della Gaspera, E.; Ou, J. Z.; Kaner, R. B.; Kalantar-zadeh, K.; Daeneke, T. Excitation Dependent Bidirectional Electron Transfer in Phthalocyanine-Functionalised MoS_2 Nanosheets. *Nanoscale* **2016**, *8*, 16276−16283.
(14) Atkin, P.; Daeneke, T.; Wang, Y.; Carey, B. J.; Berean, K. J.; Clark, R. M.; Ou, J. Z.; Trinchi, A.; Cole, I. S.; Kalantar-zadeh, K. 2D WS_2 /Carbon Dot Hybrids with Enhanced Photocatalytic Activity. *J. Mater. Chem. A* **2016**, *4*, 13563−13571.
(15) Tilmann, R.; Weiß, C.; Cullen, C. P.; Peters, L.; Hartwig, O.; Höltgen, L.; Stimpel-Lindner, T.; Knirsch, K. C.; McEvoy, N.; Hirsch, A.; Duesberg, G. S. Highly Selective Non-Covalent On-Chip Functionalization of Layered Materials. *Adv. Electron. Mater.* **2021**, *7*, 2000564.
(16) Canton-Vitoria, R.; Stangel, C.; Tagmatarchis, N. Electrostatic Association of Ammonium-Functionalized Layered-Transition-Metal Dichalcogenides with an Anionic Porphyrin. *ACS Appl. Mater. Interfaces* **2018**, *10*, 23476−23480.
(17) Luo, C.-Y.; Huang, W.-Q.; Hu, W.; Peng, P.; Huang, G.-F. Non-Covalent Functionalization of WS_2 Monolayer with Small Fullerenes: Tuning Electronic Properties and Photoactivity. *Dalton Trans.* **2016**, *45*, 13383−13391.
(18) Zhou, C. J.; Yang, W. H.; Wu, Y. P.; Lin, W.; Zhu, H. L. Theoretical Study of the Interaction of Electron Donor and Acceptor Molecules with Monolayer WS_2. *J. Phys. D: Appl. Phys.* **2015**, *48*, 285303.
(19) Marcia, M.; Singh, P.; Hauke, F.; Maggini, M.; Hirsch, A. Novel EDTA-Ligands Containing an Integral Perylene Bisimide (PBI) Core as an Optical Reporter Unit. *Org. Biomol. Chem.* **2014**, *12*, 7045−7058.
(20) Huang, C.; Barlow, S.; Marder, S. R. Perylene-3,4,9,10-Tetracarboxylic Acid Diimides: Synthesis, Physical Properties, and Use in Organic Electronics. *J. Org. Chem.* **2011**, *76*, 2386−2407.
(21) Marcia, M.; Hirsch, A.; Hauke, F. Perylene-Based Non-Covalent Functionalization of 2D Materials. *FlatChem* **2017**, *1*, 89−103.
(22) Sideri, I. K.; Jang, Y.; Garcés-Garcés, J.; Sastre-Santos, Á.; Canton-Vitoria, R.; Kitaura, R.; Fernández-Lázaro, F.; D'Souza, F.; Tagmatarchis, N. Unveiling the Photoinduced Electron-Donating Character of MoS_2 in Covalently Linked Hybrids Featuring Perylenediimide. *Angew. Chem., Int. Ed.* **2021**, *60*, 9120−9126.
(23) Wilson, J. A.; Yoffe, A. D. The Transition Metal Dichalcogenides Discussion and Interpretation of the Observed Optical, Electrical and Structural Properties. *Adv. Phys.* **1969**, *18*, 193−335.
(24) Lin, Y.; Ling, X.; Yu, L.; Huang, S.; Hsu, A. L.; Lee, Y.-H.; Kong, J.; Dresselhaus, M. S.; Palacios, T. Dielectric Screening of Excitons and Trions in Single-Layer MoS_2. *Nano Lett.* **2014**, *14*, 5569−5576.
(25) Synnatschke, K.; Cieslik, P. A.; Harvey, A.; Castellanos-Gomez, A.; Tian, T.; Shih, C.-J.; Chernikov, A.; Santos, E. J. G.; Coleman, J. N.; Backes, C. Length- and Thickness-Dependent Optical Response of Liquid-Exfoliated Transition Metal Dichalcogenides. *Chem. Mater.* **2019**, *31*, 10049−10062.
(26) Berkdemir, A.; Gutiérrez, H. R.; Botello-Méndez, A. R.; Perea-López, N.; Elías, A. L.; Chia, C.-I.; Wang, B.; Crespi, V. H.; López-Urías, F.; Charlier, J.-C.; Terrones, H.; Terrones, M. Identification of Individual and Few Layers of WS_2 Using Raman Spectroscopy. *Sci. Rep.* **2013**, *3*, 1755.
(27) Gutiérrez, H. R.; Perea-López, N.; Elías, A. L.; Berkdemir, A.; Wang, B.; Lv, R.; López-Urías, F.; Crespi, V. H.; Terrones, H.; Terrones, M. Extraordinary Room-Temperature Photoluminescence in Triangular WS_2 Monolayers. *Nano Lett.* **2013**, *13*, 3447−3454.
(28) Liu, X.; Gu, J.; Ding, K.; Fan, D.; Hu, X.; Tseng, Y.-W.; Lee, Y.-H.; Menon, V.; Forrest, S. R. Photoresponse of an Organic Semiconductor/Two-Dimensional Transition Metal Dichalcogenide Heterojunction. *Nano Lett.* **2017**, *17*, 3176−3181.
(29) Kohl, C.; Weil, T.; Qu, J.; Müllen, K. Towards Highly Fluorescent and Water-Soluble Perylene Dyes. *Chem. - Eur. J.* **2004**, *10*, 5297−5310.
(30) Long, S.; Wang, Y.; Vdović, S.; Zhou, M.; Yan, L.; Niu, Y.; Guo, Q.; Xia, A. Energy Transfer and Spectroscopic Characterization of a Perylenetetracarboxylic Diimide (PDI) Hexamer. *Phys. Chem. Chem. Phys.* **2015**, *17*, 18567−18576.
(31) Canton-Vitoria, R.; Scharl, T.; Stergiou, A.; Cadranel, A.; Arenal, R.; Guldi, D. M.; Tagmatarchis, N. Ping-Pong Energy Transfer in Covalently Linked Porphyrin-MoS_2 Architectures. *Angew. Chem., Int. Ed.* **2020**, *59*, 3976−3981.

https://doi.org/10.1021/jacs.1c11977
J. Am. Chem. Soc. 2022, 144, 5834−5840

(32) Wibmer, L.; Lages, S.; Unruh, T.; Guldi, D. M. Excitons and Trions in One-Photon- and Two-Photon-Excited MoS_2 : A Study in Dispersions. *Adv. Mater.* **2018**, *30*, 1706702.
(33) Bonchio, M.; Syrgiannis, Z.; Burian, M.; Marino, N.; Pizzolato, E.; Dirian, K.; Rigodanza, F.; Volpato, G. A.; la Ganga, G.; Demitri, N.; Berardi, S.; Amenitsch, H.; Guldi, D. M.; Caramori, S.; Bignozzi, C. A.; Sartorel, A.; Prato, M. Hierarchical Organization of Perylene Bisimides and Polyoxometalates for Photo-Assisted Water Oxidation. *Nat. Chem.* **2019**, *11*, 146−153.

https://doi.org/10.1021/jacs.1c11977
J. Am. Chem. Soc. 2022, 144, 5834−5840